Cation-controlled permeation of charged polymers through nanocapillaries

Fahim Faraji [1,2,3,*] Mehdi Neek-Amal [2,4,†] Erik C. Neyts [1,3,‡] and François M. Peeters [2,3,5,§]

[1]*PLASMANT, Department of Chemistry, University of Antwerp, Universiteitsplein 1, 2610 Antwerp, Belgium*
[2]*Condensed Matter Theory, Department of Physics, University of Antwerp, Groenenborgerlaan 171, 2020 Antwerp, Belgium*
[3]*Center of Excellence NANOlab, University of Antwerp, Groenenborgerlaan 171, 2020 Antwerp, Belgium*
[4]*Department of Physics, Shahid Rajaee Teacher Training University, 16875-163 Tehran, Iran*
[5]*Departamento de Física, Universidade Federal do Ceará, Fortaleza-CE 60455-760, Brazil*

(Received 28 May 2022; revised 7 February 2023; accepted 28 February 2023; published 17 March 2023)

Molecular dynamics simulations are used to study the effects of different cations on the permeation of charged polymers through flat capillaries with heights below 2 nm. Interestingly, we found that, despite being monovalent, Li^+, Na^+, and K^+ cations have different effects on polymer permeation, which consequently affects their transmission speed throughout those capillaries. We attribute this phenomenon to the interplay of the cations' hydration free energies and the hydrodynamic drag in front of the polymer when it enters the capillary. Different alkali cations exhibit different surface versus bulk preferences in small clusters of water under the influence of an external electric field. This paper presents a tool to control the speed of charged polymers in confined spaces using cations.

DOI: 10.1103/PhysRevE.107.034501

I. INTRODUCTION

Charged polymers are prevalent in nature and industry. They can be produced when polyelectrolytes dissociate. Polyelectrolytes have ionizable functional groups. Upon dissolution of polyelectrolytes in water, the ionizable groups will dissociate, and while dispersing counter ions in the water, polyelectrolytes will turn into charged polymers. DNA and most proteins are examples of these macromolecules [1]. The highly solvable characteristics of charged polymers make them beneficial to a wide range of industrial applications, including drug delivery [2–4], nanoreactors [5,6], and cell biology [7,8].

Experiments have revealed the entropically driven movement of polyelectrolytes when they tend to become unstructured, which motivates the study of charged polymers inside confinement [9]. Furthermore, through the translocation inside nanoscale spaces, charged polymers can be detected, processed, and sequenced [10–13]. Nanocapillaries at molecular scales have been made possible due to recent advances in fluidics fabrication [14–24]. The slit pores of few molecular diameters provide enhanced control over confinement [25]. Due to this, they have attracted a lot of attention. In highly confined capillaries, how the polymer attempts to permeate the capillary might have just as much influence on its transmission as the behavior of the polymer inside the capillary itself. Earlier studies conducted on macromolecules' translocation were mostly limited to spaces of the order of 10 nm and beyond [26–28]. Here we investigate a very different regime with polymer transmission in narrow capillaries below 2 nm.

Conventional theories such as the de Gennes regime [29], the Odijk regime [30], Manning [31], and Poisson-Boltzmann [32] might not be applicable in strong confinements, and furthermore they do not consider the details of ionic interaction and the specificity of counterions. Molecular simulations do not have those restrictions. We used molecular dynamics (MD) simulation to investigate how different cations of Li^+, Na^+, and K^+ influence the permeation of a charged polymer through a capillary with a 1.8-nm height. Since C and H atoms are ubiquitous constituents of charged polymers, we used a hydrocarbon molecule ($C_{10}H_{22}$) with an artificial electrical charge on its atoms as a representative of a charged polymer. This particular polymer molecule was chosen to have a characteristic size comparable and smaller than the capillary size so it will not feel an entropic barrier when it is permeating through the capillary. Interestingly, we found that the aforementioned cations, although being monovalent, had different influences on the polymer permeation. This, in turn, affected the dynamics of the polymer when transmitted inside the capillary. Our paper shows that the permeation and transmission speeds of charged polymers in confined capillaries can be modulated by varying the type of cation.

II. THE MODEL

The simulation system is schematically shown in Fig. 1. The system consists of two reservoirs connected by a narrow capillary made of two graphene sheets. The reservoirs are filled with water with a bulk density of 1000 kg/m^3. KCl, LiCl, and NaCl are used as electrolytes which are dispersed inside the reservoirs. The polymer initially was put in the corner of the feed (left) reservoir. The reservoirs' dimensions

*fahim.faraji@uantwerpen.be
†mehdi.neekamal@gmail.com
‡erik.neyts@uantwerpen.be
§francois.peeters@uantwerpen.be

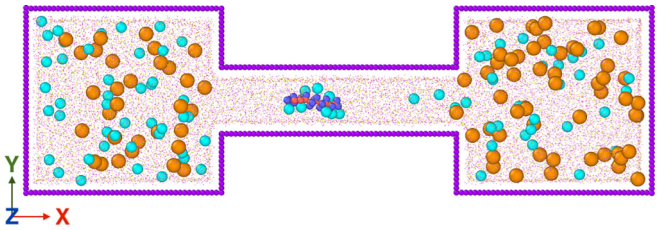

FIG. 1. Schematic of the simulation setup. The feed and permeate reservoirs are connected by a narrow flat capillary. External electrical field is applied on the charged particles pulling a negatively charged polymer from the feed reservoir into the capillary and subsequently it diffuses into the permeate reservoir. Cyan and orange particles represent cations (K^+, Na^+, Li^+) and anions (Cl^-), respectively. For ease of illustration, water molecules are depicted as tiny points.

are 5.3 nm × 5.3 nm × 5.0 nm, assuring enough space to accommodate ample ions up to 1 M concentration. The capillary length is 6.3 nm having a height of 1.8 nm. Periodic boundary condition is applied along the z direction.

Each polymer atom was given an artificial electric charge of −0.5e. The system's atoms feel an applied body force proportional to their charge, which is similar to the case of a uniform electrical field. When the polymer is exposed to the electric field, it starts permeating through the capillary. The direction of the electrical field was set such that it pulls the negatively charged polymer into the capillary and the permeate (right) reservoir.

III. RESULTS AND DISCUSSION

Figures 2(a)–2(d) show the time-displacement curves of the polymer center of mass for four different applied electrical fields, which are equivalent to applying voltages of, respectively, 5 V, 12 V, 25 V, and 50 V across the entire system. For each case, calculations were performed with five different KCl concentrations. Note that the polymer encounters a barrier

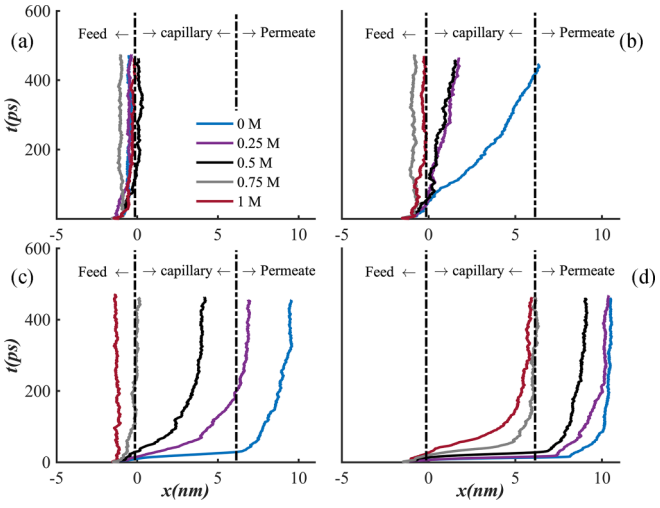

FIG. 2. Time evolution of the polymer center of mass for five different KCl ion concentrations subjected to different voltages across the system: 5 V(a), 12 V(b), 25 V(c), and 50 V (d).

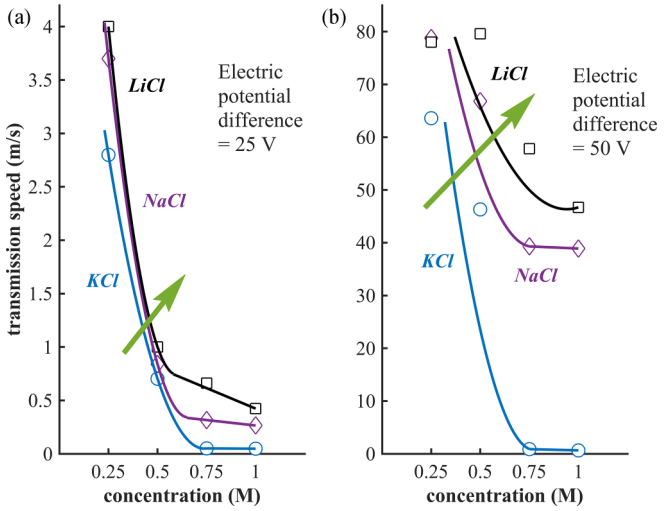

FIG. 3. Polymer mean velocity inside the capillary versus the cation concentration for KCl, NaCl and LiCl electrolytes at 25 V (left) and 50 V (right). The curves are guide to the eye.

when trying to permeate through the capillary. For instance, for the lowest voltage (5 V) we observe that for all KCl concentrations, the polymer moves toward the capillary mouth but is not able to enter the capillary. In the following, we will examine the origins of such an entry barrier. For larger voltages, the KCl concentration within the reservoirs influences the polymer transmission considerably: The smaller the KCl concentration, the larger the polymer entry probability, and the faster the polymer transmission.

The probability of permeation and transmission speed are higher for larger voltages, as one would expect (see Fig. 2). However, it is intriguing that polymer transmission speed correlates inversely with reservoir ion concentration. This is similar to what occurs in DNA translocation through nanopores with heights of about 10 nm [33]. Therefore, we may hypothesize that the countercations (K^+ here) which have settled on the polymer surface reduced its effective charge and in doing so reduces the effective force acting on the polymer.

To explore further, additional simulations were performed using LiCl and NaCl electrolytes as well. The time-displacement curves of Li^+ and Na^+ as cations are depicted in Supplemental Material Figs. S1 and S2, respectively [34]. Li^+ and Na^+ cases also exhibit suppression of transmission at higher concentrations, although the curves for different cations are not the same. Note that similar results were observed earlier in DNA experiments, showing that although potassium, lithium, and sodium are all monovalent cations, their impact on transmission is different [33].

Figure 3 illustrates the polymer transmission mean velocities for different electrolytes and concentrations at 25 V and 50 V. The mean velocity of polymer was found by fitting a line to the time-displacement curves when polymer is inside the capillary. Interestingly, different cations result in different polymer transmission velocities with the largest for lithium and the smallest for potassium. The trend is in contrast to the observation of DNA translocation in nanopores, where translocation was slowed when potassium ions were replaced by lithium [33].

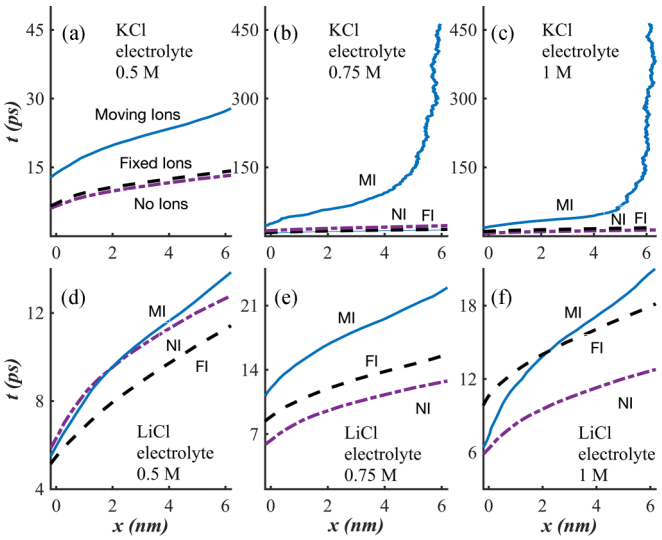

FIG. 4. Polymer time-displacement curves for three different systems including without ions, with ions, and with ions frozen at particular positions. The upper and lower rows, respectively, are for KCl and LiCl electrolytes, and the columns from left to right are for 0.5 M, 0.75 M and 1 M solute concentrations.

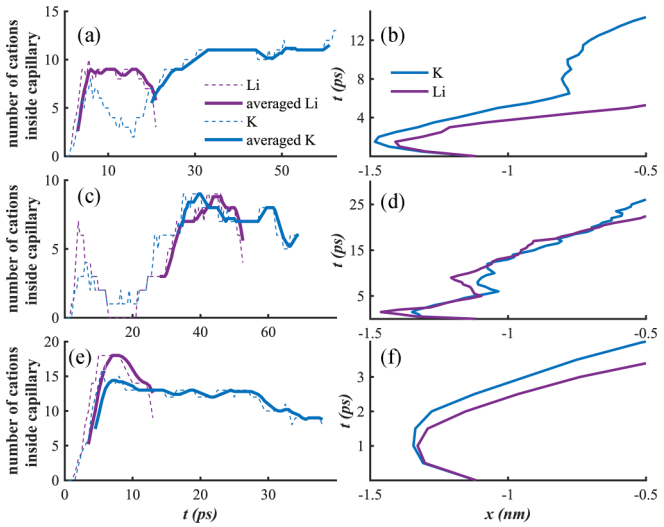

FIG. 5. (a) Number of cations inside the capillary of height 1.8 nm for potassium and lithium electrolytes versus time. The curves at the time intervals in which the polymer resides inside the capillary are bolded. (b) Time-displacement curves. The capillary gave a bias to lithium electrolyte in a way that the polymer in potassium electrolyte felt a barrier when entering the capillary. Panels (c), (d) and (e), (f) are the same quantities as (a), (b), respectively, for capillaries of height 1.4 nm and 2.4 nm. In the 1.4 nm capillary, the polymer felt a barrier in both cases while for the 2.4 nm capillary there is no entrance barrier.

To investigate further, we examined the time-displacement curves for three different cases including systems without solute ions, systems with ions, and systems with ions fixed at certain positions (generated initially at random), thus, not able to move. The latter case was investigated to determine whether the ions' influence was solely due to their attachment to the polymer surface or if they would also produce an electrophoretic barrier. Figures 4(a)–4(c) show the time-displacement curve for potassium [Figs. 4(a)–4(c)] and lithium [Figs. 4(d)–4(f)] for the three mentioned cases. For each cation, the three columns from left to right are related to ion concentrations of 0.5M, 0.75M, and 1M, respectively. Notice that the x axis is restricted to the capillary length. Clearly, when lithium is present, all three curves are relatively close to each other, whereas for potassium the curves of the systems with moving ions are separated from the other two.

In both potassium and lithium electrolytes, the fixed ion curves are very close to the curves in the absence of any ions. This is sufficient to conclude that adhesion of the cations to the surface of the polymer and, consequently, the reduction of its effective charge dominate the polymer dynamics. Nevertheless, the next question is: Why is there such a clear difference in potassium and lithium solutions? Is this related to what is happening inside the capillary or does it originate from what is happening prior the polymer enters the capillary?

Figure 5(a) shows the number of cations within the capillary for both potassium and lithium electrolytes at 50 V versus time. The start of the time was set to when the polymer started moving. The bold curves are averaged over the last 2.5 ps and are depicted for the time interval when the polymer resided inside the capillary. It is apparent that in potassium electrolyte, the number of cations inside the capillary, and consequently the number of cations settling on the polymer surface are higher than in lithium electrolyte. Thus, it is understandable why the polymer velocity was lower with potassium electrolytes (see Fig. 3). Another important point to note is that the polymer in potassium electrolyte enters the capillary much later than that in lithium electrolyte. Therefore, one can conclude that the main reason for the difference in the systems' behavior is the pre-entering of the polymers into the capillary. Figure 5(b) illustrates the time-displacement curves of the same two cases as Fig. 5(a), emphasizing the capillary mouth. The polymer enters the capillary quite smoothly in lithium electrolyte, whereas in potassium electrolyte the polymer experiences a barrier before entering the capillary.

To describe these effects, we hypothesize that the aforementioned barrier is present in both potassium and lithium electrolytes; however, in potassium electrolyte, from the beginning of the polymer movement until it reaches the capillary mouth, a higher number of cations have settled on its surface than in lithium electrolyte. According to our MD trajectories, at the capillary mouth, five K^+ ions stick to the polymer in the case of potassium electrolyte, while three Li^+ ions stick to it for lithium electrolyte. Therefore, the polymer in potassium electrolyte has a lower effective charge, so the applied electrical force is less to overcome the barrier. It is for this reason that the polymer enters the capillary noticeably later in the presence of the potassium electrolyte. This delay at the capillary mouth, in turn, causes even more cations to settle on the surface of the polymer and, eventually, the polymer enters the capillary with a higher number of cations and a lower velocity. The reason why a higher number of K^+ ions stick to the polymer before it enters the capillary than Li^+ ions can be attributed to the higher hydration strength of the lithium ions (hydration enthalpy of -520 kJ/mol for lithium as opposed to -322 kJ/mol for potassium [35]). If the ions are to settle

on the polymer surface, they need to be dehydrated (at least partially), which is more likely for potassium ions.

To examine this hypothesis, we repeated the simulations for two different capillary heights of 1.4 nm and 2.4 nm, where we expect higher and lower entrance barriers, respectively. Figure 5(c) depicts the number of cations for the 1.4 nm capillary. For both electrolytes, the number of cations inside the capillary is about the same, and the polymer enters the capillary almost simultaneously. Figure 5(d) illustrates the time-displacement curves of the 1.4 nm capillary emphasizing the capillary mouth. Contrary to the 1.8 nm capillary, here the barrier is also pronounced for the lithium electrolyte. Due to the narrower capillary, the barrier will be even larger, causing the polymer in lithium electrolyte also to be held up at the capillary mouth for some time, and eventually its dynamics will be close to the case of potassium electrolyte. Our MD trajectories show that at the capillary mouth, six cations stick to the polymer for both electrolytes.

Figures 5(e) and 5(f) illustrate the number of cations inside the capillary and the time-displacement curves emphasising the capillary mouth for the 2.4 nm capillary, respectively. The capillary is wider this time, and the barrier is not pronounced for any of the systems [see Fig. 5(f)]. This is why in Fig. 5(e) the polymer enters the capillary almost simultaneously for both electrolytes. Despite this, Fig. 5(e) shows that a larger number of Li^+ ions are present in the capillary. The MD trajectories indicate that those are dispersed ions that enter the capillary due to the capillary's large height (we did not detect them in 1.4 nm and 1.8 nm capillaries). At the capillary mouth, three cations stick to the polymer for both electrolytes. There is still a possibility that some of the dispersed ions inside the capillary may stick to the polymer. The number of such cations is higher in potassium electrolytes, again due to its lower hydration energy. This is why the polymer stays in the capillary much longer for potassium electrolyte than for lithium electrolyte [see Fig. 5(e)].

The Supplemental Material Figs. S3 and S4 [34] illustrate the time-displacement curves of the polymer for the 1.4 nm and 2.4 nm capillaries. For both figures, the corresponding profiles of the 1.8 nm capillary are also shown for comparison. For the 1.8 nm capillary, where the capillary mouth barrier gave a bias to one of the cation types, the curves are diverging, while the curves for the 1.4 nm and 2.4 nm capillaries are rather close to each other.

Using the interplay of ions' hydration energies and capillary mouth barriers, one could design a system for controlling polymer velocity. Unlike the standard capillary effect, where the fluid diffuses into the capillary due to adhesion, the polymer here had to cross a barrier to enter the capillary. The capillary mouth barrier is attributed to hydrodynamic drag caused by the water inside the capillary. Indeed, when we modeled the same system without water molecules, the polymer was in a vacuum inside the geometries and moved unimpeded toward the right reservoir. Considering the very short characteristic length of the capillary, the dynamics of water inside the capillary can readily be classified as the standard creeping flow regime (Reynolds number $<< 1$). The drag force on the moving object can then be approximated by the Stokes relation ($F = 6\pi r\mu v$), where r and v refer to the radius and velocity of the object, respectively, and μ is the fluid's dynamic viscosity. Deviation from the perfect sphere geometry can be compensated using correction coefficients. Thus, we are able to identify the direct effect of the viscosity of water on the drag force felt by the polymer. Water within highly confined capillaries has been shown to exhibit solidlike properties with a threefold increase in viscosity compared to bulk water [36,37]. Therefore, it is expected for the polymer to encounter a noticeable barrier when permeating through the capillary. At this point, we are able to explain the contradiction between our results and the DNA experiment [33] concerning the trend for cations' influences. In the DNA experiment, the molecule does not experience a significantly enhanced hydrodynamic drag at the pore opening as compared when inside the reservoir. Furthermore, given the experiment's timescale (milliseconds), the cations had ample time to bond with the DNA, so they could simply be regulated based on their interaction strength, which is considerably larger for lithium than potassium (See the Methods section below).

At this stage, we believe we should pay particular attention to the solvation of the cations. The hydration enthalpies discussed above are in fact the results of experiments involving the dehydration of ions in infinite amounts of water. In the present study, the cations are surrounded by small clusters of water. Therefore, results obtained with infinite solvents may not be valid. Additionally, in infinite solvent experiments or continuum theories of dielectrics, the free energy of dehydration is largely assumed to come from enthalpic contributions, and entropy is virtually always ignored [38–40]. In dielectric theory, Born's model estimates that entropy contributes only about 0.5% of the enthalpy contribution [41,42]. However, in studying the ions' interface solvation in small clusters of water, the entropic contribution is indeed found to be of the same order of magnitude as the enthalpy contribution [43]. It has even been proposed that the bulk hydration of small halides like F^- is driven by entropy [44].

Moreover, the water model used here is a simple charge model (see Methods section) that cannot accommodate induced polarizations, while an accurate study of ionic solvations requires polarization capabilities for both water and ions. For our purpose, which is to compare the hydration energies of K^+ and Li^+ cations, one appropriate approach would be to examine the surface versus bulk preferences of the cations in a cluster of water under conditions similar to our problem. Surface solvation analysis is useful in that it could reveal how cations prefer to sit at the interface of water and polymer [43].

In the past, interface solvation has been extensively studied, but its conclusions have changed substantially over time. A large dipole moment was initially recognized as critical [45]. Later, it was determined that induced polarization, coupled with the size and sign of ions, was the major cause of surface solvation [43]. Eventually, the absence of a single explanation for the solvation of various ions was identified [44]. Nevertheless, what is commonly concluded in the literature for alkali cations is that they all favor bulk solvation [39,46] and their hydration is entirely determined by enthalpy with a negligible contribution from entropy [44]. As a result, we may draw two conclusions. First, the energetics analysis is sufficient to compare the dehydration of potassium and lithium in our problem. Second, our simple charge water model (see Methods section) is adequate for this energetic purpose. If the

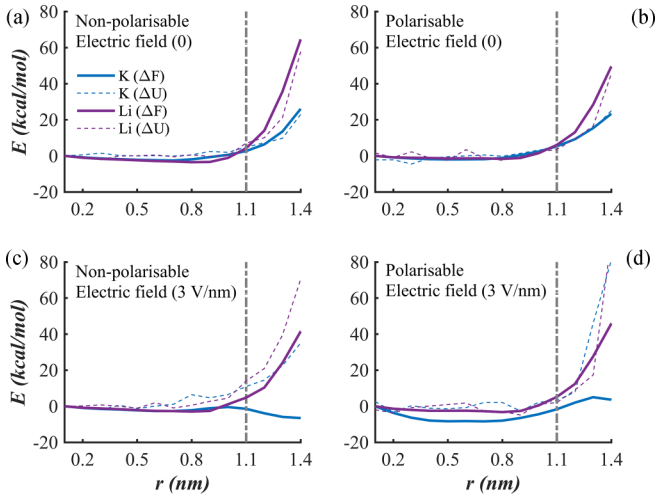

FIG. 6. Free energy (solid lines) and internal energy (dashed lines) as a function of cation distance from the water cluster center of mass for two cations, K^+ and Li^+. In the upper panels, there is no external electric field, while in the lower panels there is an external electric field of 3 V/nm. Panels on the left show results for the nonpolarizable model, while panels on the right show results for the polarizable model.

problem was related to large halide ions, which are believed to favor surface solvation, a simple charge water model might result in qualitative and quantitative inaccuracies [43].

Despite these, we still cannot conclude that our model is completely reliable. In our problem, there is a strong external electrical field (3 V/nm equivalent to 50 V for the problem geometry). This strong field, although not yet large enough to make the water conductive, would profoundly alter the solvation and screening properties; even making differences specific to different ions. As far as we are aware, interface solvation has not been fully investigated in the literature in the presence of an external electric field. Therefore, we conducted a steered molecular dynamics (SMD) investigation for the solvation of K^+ and Li^+ cations within a spherical cluster of water (with 1.1 nm radius) containing 186 water molecules, the same order of magnitude as the ratio of the amount of water to the amount of cations found in our reservoirs (see Methods section for details about the simulations). Simulations were conducted for two different situations, without an electric field and with an electric field of 3 V/nm. Each case is repeated for two water models: The nonpolarizable simple charge SPC/E model [47] (similar to our other simulations), and the ReaxFF model [48,49] which is capable of polarizing both water and cations.

The results are shown in Fig. 6. The figures display the free energy (potential of mean force) and potential energy of the system as function of the distance between the cation and the cluster's center of mass. During SMD simulations, a canonical ensemble (NVT) has been sampled, which indicates that the Helmholtz free energy represents the thermodynamics potential. Details of calculating the free energy are described in the Methods section. The potential energy is determined by summing the van der Waals, electrostatic, and polarization energies of all species. By neglecting the changes in the system's kinetic energy, the potential energy represents the system's total energy. By subtracting the curves, we can calculate the entropic contribution $TdS(r) = dU(r) - dF(r)$. As water molecules are electrically neutral, the external electric field will not impose any pressure gradients within the system. Additionally, the simulations are performed at a constant temperature. Therefore, we assume that discussing the problem within the framework of equilibrium thermodynamics is relevant.

In the absence of an electric field, as expected, both K^+ and Li^+ cations favor bulk solvation as predicted by both polarizable and nonpolarizable models. Additionally, the free energy and energy curves are close to each other, suggesting a subtle role for entropy, as expected. Furthermore, Li^+ has a higher solvation energy than K^+ when the cations are moving away from the cluster. Continuing the free curves to larger radiuses (for example, $r > 2.5$ nm), the curves would approach plateau horizontal behavior, which would express the total free energy of desolvation, which is larger for Li^+ than for K^+. More importantly, for either the absence or the presence of electric field, the results of the polarizable and non-polarizable models are quite similar. Therefore, we expect that our simple charge SPC/E model has been reliable for this study.

An interesting observation from the curves when an electric field is present is that potassium favors surface solvation while lithium does not. In turn, this strengthens our hypothesis that K^+ cations are more readily dehydrated than Li^+ cations and settle on the surface of the polymer. As a result, K^+ cations are more easily dehydrated than Li^+ cations, not only due to their lower hydration energy but also because of a weakening and partial unoccupation of the hydration shells, which occurs for potassium but not for lithium due to strong electric fields [50]. These results indicate that alkali cations exhibit different surface versus bulk preferences when an electric field is present, depending on their interactions with the solvent species. It is similar to the behavior of cations in dimethyl sulfoxide (DMSO) solvent [51], in which the hydration of larger alkalis, which bond less strongly to the solvent, weakens more than the hydration of small ions when present in strong electric fields (same order of magnitude as in our study).

Potassium's surface solvation has occurred in such a manner that its energy curve still continues to increase monotonously. This indicates that it is entropy that has brought the cation to the surface. Since both polarizable and nonpolarizable models exhibit the same behavior, this suggests that surface solvation does not result from polarization (as has been established for large halides [43,44]) but rather from the alignment of the dipoles of the water molecules in the direction of the electric field and the perturbation of the hydrogen bond network [50]. When all dipoles are parallel, the entropy of the system is minimal (similar to the concept of freezing in dielectrics [43]). When the K^+ cation is located close to the center of the cluster, its dipole will also orient itself according to the dipoles of the water molecules. As the K^+ cation approaches the surface, it feels agile and perturbs its surrounding dipoles and hydrogen bonds, resulting in an increase in entropy. Due to the strong bond between the Li^+ cation and water, its freedom will not increase that much when it comes to the surface, so no substantial increase in entropy is observed.

In addition, we analyzed a hypothetical scenario using our simple charge SPC/E model for potassium in the presence of an electric field, changing the partial charges of the water atoms to increase the dipole of the molecule from 2.35D (as per the SPC/E model) to 2.6 D. The obtained free energies were almost unchanged, indicating that it is not the magnitude of the dipoles but their alignment that drives the K^+ cation to the surface. With a simple comparison of the hydration enthalpies of potassium and lithium, we were able to accurately assess the true trend to build our hypothesis. Nevertheless, calculating the free energy still strengthens the hypothesis. This is analogous to the pure energetics analysis for interface solvation of halides (with a polarizable force field), which, although quantitatively not quite precise, can qualitatively predict surface versus bulk preference [43].

We have employed ReaxFF parameterized for electrolyte solutions (available in the supplementary information of Ref. [52]) with the standard Qeq charge distribution model [53]. Considering that even the simple charge model has similar predictions as the polarizable model (see Fig. 6), the method of charge polarization should not have a significant impact. In the presence of an external electric field, Qeq may impose an unphysical charge distribution due to its global charge transfer across the simulation domain [54]. It has been shown that atom-condensed Kohn-Sham density functional theory (DFT) approximated to second-order (ACKS2) is able to overcome the shortcomings of Qeq [54]. Nevertheless, the unphysical gradient of charge density in a NVT MD simulation with Qeq for a water cluster is several orders of magnitude smaller than that of our problem of attracting cations to the polymer by electrostatic forces [54]. Therefore, we have used the widely used Qeq charge distribution for which ReaxFF has already been examined for electrolyte solutions.

We performed a few additional simulations to investigate whether, in addition to the hydrodynamic drag, there is also an energy barrier in front of the polymer when it enters the capillary. Additionally, we were also able to gain a direct understanding of the changes in hydrodynamic drag, confirming predictions based on an increase in viscosity. This may be more straightforward than calculating the viscosity because, on the one hand, the passage of the polymer inside the capillary causes the problem to be mechanically nonequilibrium, preventing equilibrium calculation of the viscosity. Taking a nonequilibrium approach to the problem, on the other hand, it is unclear whether the liquid with the polymer inside will behave as a Newtonian fluid so a shear flow can be applied externally and the velocity gradient measured. The polymer was placed into the left reservoir horizontally along the capillary axis. Then, we moved the polymer toward the capillary mouth at a constant velocity of 2 Å/ps, and calculated the horizontal component of the force exerted on the polymer, as well as the potential energy of the system (see Supplemental Material Fig. S5 [34]). At the capillary mouth, the force increases clearly, illustrating the existence of a hydrodynamic drag barrier. As expected, this increase is the largest for the 1.4 nm capillary and the smallest for the 2.4 nm capillary. The potential energy curves are nevertheless nearly uniform, indicating that there is no energy barrier in front of the polymer as it enters the capillary.

Further, one can compare the free energy ($F = E - TS$) of the polymer inside the reservoir and inside the capillary. The energy curves (Supplemental Material Fig. S5 [34]) represent the enthalpic contribution (E), which is nearly equal for the reservoir and capillary, provided that the polymer is horizontal. This is the case for our application, as the polymer was horizontal at the capillary mouth when it attempted to penetrate the capillary. We estimate the polymer's entropy (S) as $k_B lnN$, where k_B is the Boltzmann constant and N is the number of configurations it can adopt [55]. In an in-line configuration, the polymer length is around 14.2 Å (plus 3.4 Å for C-C distances on both sides. See the Methods section below.). Furthermore, its gyration radius can be estimated as 4.22 nm, which can be calculated discretely as the root mean square distance of the polymer atoms (weighted by particle mass) with respect to the polymer center of mass ($[\Sigma_{i=1}^{n} m_i r_i^2 / \Sigma_{i=1}^{n} m_i]^{1/2}$, m_i and r_i being the particle mass and the particle distance to the center of mass, respectively). In comparison to the channel height (1.8 nm), it is not inconceivable to envisage as many plausible configurations for the polymer inside the capillary as inside the reservoir. Consequently, the polymer enters the capillary with no free energy barrier, and thus the total contribution is attributed to the hydrodynamic drag.

As a result of the applied electrical field, the entire simulation domain will become polarized. Polarization decreases the strength of the electrical field, which depends on the amount of added ions and may vary as the polymer moves. It was necessary to examine the capillary's ability to sort out different ions, giving some preference over others, at this stage to determine whether the effect of polarization in the different electrolytes was significant. Hence, we simulated the same system with the 1.8-nm-wide capillary without the polymer and at our highest voltage (50 V) and ions concentration (1 M).

While Cl^- anions did not exhibit any noticeable differences in permeation between potassium and lithium electrolytes, K^+ cations tended to penetrate into the capillary from the permeate reservoir slightly more than Li^+ cations (see Supplemental Material Fig. S6 [34]). Additionally, Li^+ ions are slightly more abundant inside the capillary than K^+ ions. This is because once the system has reached a steady state, the Li^+ ions tend to return to the capillary more readily from the feed reservoir than the K^+ ions. Due to these two events, the number of K^+ ions is partly larger in the feed reservoir than Li+ ions (see Supplemental Material Fig. S6 [34]).

We estimated the electric potential induced by polarization assuming that the ions were located at the center of the reservoirs (see Supplemental Material Fig. S7 [34]). Inset (right side) illustrates the difference between the voltages of the two electrolytes. The induced voltage for potassium electrolyte is partially larger, but the difference between the voltages is around 1.36 V. From the beginning of the polymer's movement until it reaches the capillary mouth, the polarization voltage is in the range from 4–6 V with a 1.3 V difference (see inset on left), which is the most relevant part of the polymer movement for us.

The same analysis is carried out with the polymer present. With the polymer at the capillary mouth, the difference between the induced voltages of the two electrolytes was 0.6 V larger than without the polymer (similarly with a higher voltage for the potassium electrolyte). This can also be attributed

to the tendency of cations to adhere to the polymer (with K^+ ions slightly more). Eventually, when compared with the field voltage (50 V), the induced voltages caused by polarization can be ignored in the interpretation of the main results.

The radial distribution function (RDF) can be used to better understand ionic and polymer solvation, as shown in Supplemental Material Fig. S8 [34]. In the main figure, RDF graphs are shown for potassium oxygen and lithium oxygen, each for two cases of inside the reservoir and inside the capillary. There is almost no difference between the two graphs, indicating that the capillary (here 1.8 nm) is not too thin to tear off the hydration shells of the cations. The first minimum for lithium is almost zero for a considerable distance, which implies that its first hydration shell is still present [56]. The coordination number of potassium and lithium (up to the first minimum of the RDFs) is 6.3 and 4, respectively, consistent with the literature [57]. Therefore, our LJ model, in conjunction with electrostatic forces, appropriately models their hydration (see inset at left).

The other three curves shown in the left inset along with their corresponding RDF graphs (right inset) represent the polymer solvation (polymer-O), as well as the distance between the polymer's heavy atom (here C) and the cations (polymer-K and polymer-Li). It is apparent from the location of the first peak in the RDF graphs (right inset) or, alternatively, from the point at which coordination numbers begin to rise (left inset), that the cations have penetrated well into the polymer's first hydration shell. This also demonstrates the partial dehydration of the cations.

Lastly, we address the water structure near the hydrophobic graphene walls. We calculated the number density of oxygen and hydrogen atoms next to the capillary wall with and without the polymer inside (see Supplemental Material Fig. S9 [34]). The number density of hydrogen in half value is shown in the figure. As the first peak value for hydrogen is almost coincidentally 1.5 times larger than for oxygen, we can deduce that the structure of water molecules near the graphene is almost evenly populated between dangling OH groups and the two hydrogen atoms facing the wall, indicating moderate hydrogen bonds among the water molecules. The graphs indicate that the polymer has little impact on the water structure, although slightly denser water molecules are found close to the wall when the polymer is present.

IV. CONCLUSION

We studied the permeation of a charged polymer driven by an external electrical field through a graphene capillary. The polymer encounters a hydrodynamic barrier while going through the capillary. In the presence of cations inside the feed reservoir, some cations adhere to the surface of the polymer. As a result, the polymer's effective charge decreases. This weakens its ability to overcome the barrier and enter the capillary. Interestingly, the monovalent cations of Li^+, Na^+, and K^+ show a different influence in a way that the polymer entering occurs more likely and the transmission speed is faster when lithium electrolyte is present, followed by sodium and then potassium electrolytes. This phenomenon is explained by the different hydration free energies of the cations. Based on their interaction strength with the solvent, different alkali cations exhibit different surface versus bulk preferences in small clusters of water when exposed to a strong external electric field. This paper shows that by exploring the interplay between the hydrodynamic barrier resulting from confinement and the electrolyte conditions, one can control the polymer transmission in nm-scale capillaries.

TABLE I. Parameters for the interaction potentials.

Atom type	σ_i (Å)	ϵ_i(kcal/mol) × 10^3	Ref.
C (decane)	3.50	65	[59]
H (decane)	2.49	30	[59]
O (water)	3.12	169	[67]
H (water)	0	0	[68]
C (graphene)	3.41	55	[69]
K	3.31	99	[70]
Na	2.58	99	[70]
Li	1.51	166	[70]
Cl	4.40	99	[70]

V. METHODS

The simulations were carried out using the LAMMPS package [58]. The water molecules were modeled using the SPC/E model. The ions were considered point-charged particles. Van der Waals interactions were modeled using the Lennard-Jones (LJ) potential, and the OPLS [59] force field was used to describe the bond, angle, and dihedral potentials of the hydrocarbon molecule. Table I summarizes the LJ coefficients, while for cross parameters Lorentz-Bertholet mixing rules were applied. Van der Waals interactions were cut off at 9.8 Å and the long-range electrostatic interactions were calculated by utilizing the particle-particle particle-mesh (pppm) algorithm in k space [60]. To accelerate the simulations, bonds and angles constraints were applied to the water molecules according to the Shake algorithm [61,62]. The Newtonian equations of motion were discretized by using the velocity-vervet algorithm with a time step of 0.5 fs. Using Nose-Hoover's thermostat (with 20 fs damping parameter), time integrations were performed in canonical ensemble (NVT) at room temperature. The initial coordinates of the particles were generated using the VMD [63] and PACKMOL [64] packages. The schematic of the simulation system (Fig. 1) was produced using OVITO software [65].

The bulk versus surface solvation of a cation (K^+ or Li^+) within a spherical cluster of water composed of 186 molecules was investigated using SMD. Free energy is calculated as described in Refs. [44,66]. The cation is bonded to a simple harmonic spring with a constant of 49 kcal · mol^{-1} $Å^{-2}$. The spring equilibrium distance from the center of mass of the cluster was gradually increased in intervals of 1 Å so the cation gradually moved from the center to the surface. In each interval, the system is initially relaxed for 50 ps, and then an NVT simulation is performed for 5 ns at room temperature and the average force felt by the spring is calculated. The free energy can be calculated by numerically integrating the force versus the distance.

The simulations were repeated using two models, one nonpolarizable and one polarizable. For the nonpolarizable

model, a simple point charge model is used for water (SPC/E) and cations (similar to that used for the main results), together with LJ and Coulomb forces. The polarizable model is based on the ReaxFF parameterised for electrolyte solutions together with the standard Qeq charge distribution. The cutoff radius for SMD simulations is taken large, i.e., 10 nm. To avoid evaporation of water molecules from the surface of the cluster, an illusory spherical wall with a radius of 1.4 nm was considered around the cluster, interacting only with water molecules according to the LJ formula (with oxygen parameters). However, the energy contributions from the interaction with the wall are not included in the calculation of energy. The other simulation details are similar to those for the main MD simulations.

ACKNOWLEDGMENTS

Part of this work was supported by FWO (Project No. G099219N). The computational resources used in this work were provided by the HPC core facility CalcUA of the Universiteit Antwerpen, and VSC (Flemish Supercomputer Center), funded by the Research Foundation Flanders (FWO) and the Flemish Government.

[1] D. Qu, J. S. Pedersen, S. Garnier, A. Laschewsky, H. Möhwald, and R. v. Klitzing, Effect of polymer charge and geometrical confinement on ion distribution and the structuring in semidilute polyelectrolyte solutions: Comparison between AFM and SAXS, Macromolecules **39**, 7364 (2006).

[2] K. A. Black, D. Priftis, S. L. Perry, J. Yip, W. Y. Byun, and M. Tirrell, Protein encapsulation via polypeptide complex coacervation, ACS Macro Lett. **3**, 1088 (2014).

[3] N. Pippa, M. Karayianni, S. Pispas, and C. Demetzos, Complexation of cationic-neutral block polyelectrolyte with insulin and in vitro release studies, Int. J. Pharm. **491**, 136 (2015).

[4] A. Nolles, A. H. Westphal, J. A. de Hoop, R. G. Fokkink, J. M. Kleijn, W. J. van Berkel, and J. W. Borst, Encapsulation of GFP in complex coacervate core micelles, Biomacromolecules **16**, 1542 (2015).

[5] A. Kawamura, A. Harada, K. Kono, and K. Kataoka, Self-assembled nano-bioreactor from block ionomers with elevated and stabilized enzymatic function, Bioconjugate Chem. **18**, 1555 (2007).

[6] A. Harada and K. Kataoka, Pronounced activity of enzymes through the incorporation into the core of polyion complex micelles made from charged block copolymers, J. Controlled Release **72**, 85 (2001).

[7] A. A. Hyman and K. Simons, Beyond oil and water—phase transitions in cells, Science **337**, 1047 (2012).

[8] E. A. Frankel, P. C. Bevilacqua, and C. D. Keating, Polyamine/nucleotide coacervates provide strong compartmentalization of $Mg2^{+}$, nucleotides, and RNA, Langmuir **32**, 2041 (2016).

[9] J. N. Bright, M. J. Stevens, J. Hoh, and T. B. Woolf, Characterizing the function of unstructured proteins: Simulations of charged polymers under confinement, J. Chem. Phys. **115**, 4909 (2001).

[10] S. J. Heerema and C. Dekker, Graphene nanodevices for DNA sequencing, Nat. Nanotechnol. **11**, 127 (2016).

[11] J. J. Kasianowicz and S. M. Bezrukov, On 'three decades of nanopore sequencing', Nat. Biotechnol. **34**, 481 (2016).

[12] S. Howorka and Z. Siwy, Nanopores and nanochannels: From gene sequencing to genome mapping, ACS Nano **10**, 9768 (2016).

[13] F. Persson and J. O. Tegenfeldt, DNA in nanochannels—directly visualizing genomic information, Chem. Soc. Rev. **39**, 985 (2010).

[14] F. Fornasiero, H. G. Park, J. K. Holt, M. Stadermann, C. P. Grigoropoulos, A. Noy, and O. Bakajin, Ion exclusion by sub-2-nm carbon nanotube pores, Proc. Natl. Acad. Sci. USA **105**, 17250 (2008).

[15] A. Siria, P. Poncharal, A.-L. Biance, R. Fulcrand, X. Blase, S. T. Purcell, and L. Bocquet, Giant osmotic energy conversion measured in a single transmembrane boron nitride nanotube, Nature (London) **494**, 455 (2013).

[16] E. Secchi, S. Marbach, A. Niguès, D. Stein, A. Siria, and L. Bocquet, Massive radius-dependent flow slippage in carbon nanotubes, Nature (London) **537**, 210 (2016).

[17] E. Secchi, A. Niguès, L. Jubin, A. Siria, and L. Bocquet, Scaling Behavior for Ionic Transport and Its Fluctuations in Individual Carbon Nanotubes, Phys. Rev. Lett. **116**, 154501 (2016).

[18] R. H. Tunuguntla, R. Y. Henley, Y.-C. Yao, T. A. Pham, M. Wanunu, and A. Noy, Enhanced water permeability and tunable ion selectivity in subnanometer carbon nanotube porins, Science **357**, 792 (2017).

[19] S. Garaj, W. Hubbard, A. Reina, J. Kong, D. Branton, and J. Golovchenko, Graphene as a subnanometre trans-electrode membrane, Nature (London) **467**, 190 (2010).

[20] R. Joshi, P. Carbone, F.-C. Wang, V. G. Kravets, Y. Su, I. V. Grigorieva, H. Wu, A. K. Geim, and R. R. Nair, Precise and ultrafast molecular sieving through graphene oxide membranes, Science **343**, 752 (2014).

[21] T. Jain, B. C. Rasera, R. J. S. Guerrero, M. S. Boutilier, S. C. O'hern, J.-C. Idrobo, and R. Karnik, Heterogeneous sub-continuum ionic transport in statistically isolated graphene nanopores, Nat. Nanotechnol. **10**, 1053 (2015).

[22] J. Feng, M. Graf, K. Liu, D. Ovchinnikov, D. Dumcenco, M. Heiranian, V. Nandigana, N. R. Aluru, A. Kis, and A. Radenovic, Single-layer MoS_2 nanopores as nanopower generators, Nature (London) **536**, 197 (2016).

[23] S. Hong, C. Constans, M. V. Surmani Martins, Y. C. Seow, J. A. Guevara Carrio, and S. Garaj, Scalable graphene-based membranes for ionic sieving with ultrahigh charge selectivity, Nano Lett. **17**, 728 (2017).

[24] J. Abraham, K. S. Vasu, C. D. Williams, K. Gopinadhan, Y. Su, C. T. Cherian, J. Dix, E. Prestat, S. J. Haigh, I. V. Grigorieva *et al.*, Tunable sieving of ions using graphene oxide membranes, Nat. Nanotechnol. **12**, 546 (2017).

[25] W. Yang, B. Radha, A. Choudhary, Y. You, G. Mettela, A. K. Geim, A. Aksimentiev, A. Keerthi, and C. Dekker, Translocation of DNA through ultrathin nanoslits, Adv. Mater. **33**, 2007682 (2021).

[26] G. F. Schneider, S. W. Kowalczyk, V. E. Calado, G. Pandraud, H. W. Zandbergen, L. M. Vandersypen, and C. Dekker, DNA translocation through graphene nanopores, Nano Lett. **10**, 3163 (2010).

[27] A. J. Storm, C. Storm, J. Chen, H. Zandbergen, J.-F. Joanny, and C. Dekker, Fast DNA translocation through a solid-state nanopore, Nano Lett. **5**, 1193 (2005).

[28] V. V. Palyulin, T. Ala-Nissila, and R. Metzler, Polymer translocation: The first two decades and the recent diversification, Soft Matter **10**, 9016 (2014).

[29] M. Daoud and P. De Gennes, Statistics of macromolecular solutions trapped in small pores, J. Phys. **38**, 85 (1977).

[30] T. Odijk, The statistics and dynamics of confined or entangled stiff polymers, Macromolecules **16**, 1340 (1983).

[31] G. S. Manning, The molecular theory of polyelectrolyte solutions with applications to the electrostatic properties of polynucleotides, Q. Rev. Biophys. **11**, 179 (1978).

[32] R. W. Wilson, D. C. Rau, and V. A. Bloomfield, Comparison of polyelectrolyte theories of the binding of cations to DNA, Biophys. J. **30**, 317 (1980).

[33] S. W. Kowalczyk, D. B. Wells, A. Aksimentiev, and C. Dekker, Slowing down dna translocation through a nanopore in lithium chloride, Nano Lett. **12**, 1038 (2012).

[34] See Supplemental Material at http://link.aps.org/supplemental/10.1103/PhysRevE.107.034501 for time-displacement curves for the polymer at various electrolyte conditions and channel heights, estimates of hydrodynamic drag on the polymer as it enters the capillary, an analysis of polarization of the simulation system, conditions of polymer and ionic solvation, as well as water structure near capillary walls.

[35] D. W. Smith, Ionic hydration enthalpies, J. Chem. Education **54**, 540 (1977).

[36] U. Raviv, P. Laurat, and J. Klein, Fluidity of water confined to subnanometre films, Nature (London) **413**, 51 (2001).

[37] M. Neek-Amal, F. M. Peeters, I. V. Grigorieva, and A. K. Geim, Commensurability effects in viscosity of nanoconfined water, ACS Nano **10**, 3685 (2016).

[38] L. Perera and M. L. Berkowitz, Many-body effects in molecular dynamics simulations of $Na^+(H_2O)_n$ and $Cl^-(H_2O)_n$ clusters, J. Chem. Phys. **95**, 1954 (1991).

[39] L. Perera and M. L. Berkowitz, Structure and dynamics of $Cl^-(H_2O)_{20}$ clusters: The effect of the polarizability and the charge of the ion, J. Chem. Phys. **96**, 8288 (1992).

[40] L. Perera and M. L. Berkowitz, Erratum: Many-body effects in molecular dynamics simulations of $Na^+(H_2O)_n$ and $Cl^-(H_2O)_n$ clusters, J. Chem. Phys. 95, 1954 (1991), [J. Chem. Phys. **99**, 4236 (1993)].

[41] R. A. Robinson and R. H. Stokes, *Electrolyte Solutions* (Butterworths Scientific Publications, London, 1959), pp. 478–497.

[42] R. W. Gurney and R. W. Gurney, *Ionic Processes in Solution*, Vol. 5 (McGraw-Hill, New York, 1953).

[43] D. H. Herce, L. Perera, T. A. Darden, and C. Sagui, Surface solvation for an ion in a water cluster, J. Chem. Phys. **122**, 024513 (2005).

[44] C. Caleman, J. S. Hub, P. J. van Maaren, and D. van der Spoel, Atomistic simulation of ion solvation in water explains surface preference of halides, Proc. Natl. Acad. Sci. USA **108**, 6838 (2011).

[45] S. J. Stuart and B. Berne, Effects of polarizability on the hydration of the chloride ion, J. Phys. Chem. **100**, 11934 (1996).

[46] L. X. Dang, Computational study of ion binding to the liquid interface of water, J. Phys. Chem. B **106**, 10388 (2002).

[47] H. Berendsen, J. Grigera, and T. Straatsma, The missing term in effective pair potentials, J. Phys. Chem. **91**, 6269 (1987).

[48] Y. Han, D. Jiang, J. Zhang, W. Li, Z. Gan, and J. Gu, Development, applications and challenges of ReaxFF reactive force field in molecular simulations, Front. Chem. Sci. Eng. **10**, 16 (2016).

[49] T. P. Senftle, S. Hong, M. M. Islam, S. B. Kylasa, Y. Zheng, Y. K. Shin, C. Junkermeier, R. Engel-Herbert, M. J. Janik, H. M. Aktulga *et al.*, The ReaxFF reactive force-field: Development, applications and future directions, npj Comput. Mater. **2**, 15011 (2016).

[50] Z. He, H. Cui, S. Hao, L. Wang, and J. Zhou, Electric-field effects on ionic hydration: A molecular dynamics study, J. Phys. Chem. B **122**, 5991 (2018).

[51] S. Kerisit, M. Vijayakumar, K. S. Han, and K. T. Mueller, Solvation structure and transport properties of alkali cations in dimethyl sulfoxide under exogenous static electric fields, J. Chem. Phys. **142**, 224502 (2015).

[52] M. V. Fedkin, Y. K. Shin, N. Dasgupta, J. Yeon, W. Zhang, D. Van Duin, A. C. Van Duin, K. Mori, A. Fujiwara, M. Machida *et al.*, Development of the ReaxFF methodology for electrolyte-water systems, J. Phys. Chem. A **123**, 2125 (2019).

[53] A. K. Rappe and W. A. Goddard, III, Charge equilibration for molecular dynamics simulations, J. Phys. Chem. **95**, 3358 (1991).

[54] J. P. Koski, S. G. Moore, R. C. Clay, K. A. O'Hearn, H. M. Aktulga, M. A. Wilson, J. A. Rackers, J. M. D. Lane, and N. A. Modine, Water in an external electric field: Comparing charge distribution methods using ReaxFF simulations, J. Chem. Theory Comput. **18**, 580 (2022).

[55] M. Muthukumar, Entropic barrier theory of polymer translocation, in *Structure and Dynamics of Confined Polymers* (Springer, Dordrecht, 2002), pp. 227–239.

[56] S. Pratihar and A. Chandra, A first principles molecular dynamics study of lithium atom solvation in binary liquid mixture of water and ammonia: Structural, electronic, and dynamical properties, J. Chem. Phys. **134**, 024519 (2011).

[57] J. Mähler and I. Persson, A study of the hydration of the alkali metal ions in aqueous solution, Inorg. Chem. **51**, 425 (2012).

[58] S. Plimpton, Fast parallel algorithms for short-range molecular dynamics, J. Comput. Phys. **117**, 1 (1995).

[59] W. L. Jorgensen, J. D. Madura, and C. J. Swenson, Optimized intermolecular potential functions for liquid hydrocarbons, J. Am. Chem. Soc. **106**, 6638 (1984).

[60] R. Hockney and J. Eastwood, *Computer Simulations Using Particles* (McGraw-Hill, New York, 1981), Vol. 61.

[61] J.-P. Ryckaert, G. Ciccotti, and H. J. Berendsen, Numerical integration of the cartesian equations of motion of a system with constraints: Molecular dynamics of n-alkanes, J. Comput. Phys. **23**, 327 (1977).

[62] H. C. Andersen, Rattle: A "velocity" version of the shake algorithm for molecular dynamics calculations, J. Comput. Phys. **52**, 24 (1983).

[63] W. Humphrey, A. Dalke, and K. Schulten, Vmd: Visual molecular dynamics, J. Mol. Graphics **14**, 33 (1996).

[64] L. Martínez, R. Andrade, E. G. Birgin, and J. M. Martínez, PACKMOL: A package for building initial configurations for molecular dynamics simulations, J. Comput. Chem. **30**, 2157 (2009).

[65] A. Stukowski, Visualization and analysis of atomistic simulation data with ovito—the open visualization tool, Modell. Simul. Mater. Sci. Eng. **18**, 015012 (2010).

[66] A. C. Johansson and E. Lindahl, Position-resolved free energy of solvation for amino acids in lipid membranes from molecular dynamics simulations, Proteins Struct. Funct. Bioinf. **70**, 1332 (2008).

[67] Y. Wu, H. L. Tepper, and G. A. Voth, Flexible simple point-charge water model with improved liquid-state properties, J. Chem. Phys. **124**, 024503 (2006).

[68] T. Werder, J. H. Walther, R. Jaffe, T. Halicioglu, and P. Koumoutsakos, On the water- carbon interaction for use in molecular dynamics simulations of graphite and carbon nanotubes, J. Phys. Chem. B **107**, 1345 (2003).

[69] L. A. Girifalco, M. Hodak, and R. S. Lee, Carbon nanotubes, buckyballs, ropes, and a universal graphitic potential, Phys. Rev. B **62**, 13104 (2000).

[70] S. Chowdhuri and A. Chandra, Hydration structure and diffusion of ions in supercooled water: Ion size effects, J. Chem. Phys. **118**, 9719 (2003).